Synthesis of MIL-100(Fe)@Fe_3O_4 from Magnetic Zircon Mining Waste Modified by CTAB for Naphthol Dye in Water Removal

Zimon Pereiz[1*], *Yunus* Pebriyanto[2], *Oktaviani* Naulita Turnip[3], *Miranti* Maya Sylvani[1], *Karelius* Karelius[1], *Eka* Putra Ramdhani[4], *Chuchita* Chuchita[1], *Retno* Agnestisia[1], *Marvin* Horale Pasaribu [1] *and Erwin* Prasetya Toepak[1,]

[1]Department of Chemistry, Faculty of Mathematics and Natural Sciences, Universitas Palangka Raya, Palangka Raya 73111, Indonesia

[2]Department of Physics, Faculty of Mathematics and Natural Sciences, Universitas Palangka Raya, Palangka Raya 73111, Indonesia

[3]Department of Microbiology, Faculty of Medicine, Universitas Palangka Raya 73111, Indonesia

[4]Department of Chemistry Education, Faculty of Teacher Training and Education, Raja Ali Haji Maritime University 29111, Indonesia

Abstract. The synthesis of MIL-100(Fe)@Fe_3O_4 composite modified by CTAB has been reported in this study. This research begins with synthesis of magnetite (Fe_3O_4), using an iron precursor from zircon mining magnetic waste. The MIL-100(Fe)@Fe_3O_4 was composited with CTAB using a room-temperature in situ synthesis method. The MIL-100(Fe)@Fe_3O_4-CTAB composite obtained was then characterized using Fourier Transform Infrared spectroscopy and X-ray diffraction. The synthesized MIL-100(Fe)@Fe_3O_4-CTAB was then used to adsorb naphthol dye from the aqueous phase. The maximum naphthol removal was obtained at a concentration of CTAB of 0.4 M and pH of 6. The adsorption kinetics showed that the adsorption followed a pseudo second-order kinetics model, with the rate constant values for MIL-100(Fe)@Fe_3O_4-CTAB being 1,712 x 10-2 g/mg.menit, respectively. The results also showed that the adsorption isotherm of MIL-100(Fe)@Fe_3O_4-CTAB follows the Langmuir isotherm for adsorption capacities of 63,036 mg/g, respectively. The results indicate that naphthol dye can be effectively removed from the aqueous phase by using the iron content in the magnetic waste from zircon mining, which was used as a precursor for the manufacture of MIL-100(Fe)@Fe_3O_4-CTAB composite.

* Corresponding author: zimonpereiz@mipa.upr.ac.id

1 INTRODUCTION

Since being recognized by the United Nations Cultural Affairs Agency (UNESCO), Indonesia is the birthplace of batik, a global cultural legacy, and the country's batik sector has occasionally grown [1]. The cultural works of art of the Indonesian nation that have been passed down from generation to generation are at the forefront of their development. The existence of Indonesia's industry of batik occupies the categories of large, medium, small, and even household-scale industries (home industry). All categories of the batik industry require serious attention to the environmental impacts they cause [2].

High artistic value is associated with batik, a traditional cloth from Indonesia's cultural heritage [3][4]. Wax-resist dyeing is the method used to create patterned fabrics known as batik. It is a patterned fabric created by methods of synthetic dyeing [5]. Every design and motif used throughout the batik fabric has a distinct meaning and philosophy associated with the customs of every Indonesian province [4]. The "Benang Bentik" batik popular in Central Kalimantan Province has grown to be a specialty in the area [6]. "Benang" refers to a piece of white cloth in the local language, while "Bintik" denotes the design that is placed on top of the "Benang." The patterns and motifs on this batik fabric are inspired by the Dayak Ngaju tribe, who are native to Central Kalimantan. Typically, the Ngaju Dayak Community uses paintings or carvings with these patterns and motifs to perform customary ceremonies and rites [7].

Synthetic dyes are typically used for the designs and patterns on batik fabric because they produce colors that are robust, stable, and simple to obtain [8]. Sadly, synthetic dyes are nondegradable, poisonous, and carcinogenic [8][2]. Waste water can pollute the environment if it is released into environmental media without first being treated, especially in aquatic ecosystems. Elevated temperatures have the effect of reducing the dissolved oxygen (DO) content in the water, leading to the death of organisms and upsetting the equilibrium of the aquatic ecosystem. In addition, organic waste raises nitrogen levels, which result in nitrate compounds and an unpleasant odor [9]. Therefore, prolonged usage of these colors may result in negative effects on the environment and human health. About 80% of the dye remains on the fabric during the dyeing process, while the rest is thrown into the water as waste [2].

Many methods, such as reverse osmosis, photocatalysis, ion exchange, oxidation, electrochemistry, activated sludge, anaerobic and aerobic degradation, adsorption, coagulation or flocculation, and photodegradation or oxidation, have been developed by researchers to remove synthetic dyes from wastewater [2][10][11]. One option for a technique is adsorption from among the many methods because it is considered effective, efficient, easy to prepare, relatively cheap operational costs, and sensitive to various toxic substances [2][10][12].

One material that can be developed as an adsorbent is metal organic framework (MOF). MOF has characteristics that support it as an adsorbent, such as its large surface area, large volume and pore size, and high crystallinity [13]. This makes MOF superior to other porous materials such as zeolites, activated carbon, and others, so it has great potential for applications in the fields of adsorption and photocatalyst development [14].

The use of MOF adsorbents in water systems has a weakness, namely the difficulty of separating the adsorbent from liquid waste after adsorption. So far, the separation process has been

carried out by filtering, but this method is not effective because it takes a long time for the separation process, so to increase its effectiveness, it is combined with magnetite (Fe_3O_4). The purpose of this combination is to give MIL-100(Fe) magnetic characteristics. An external magnetic field can be used to quickly and readily separate MIL-100(Fe) from the aqueous phase following the adsorption procedure by virtue of its magnetic characteristics [7].

In essence, dyes are chemical substances that can adhere to materials like fabrics or surfaces to produce color [7]. Since most dyes are made of intricate organic compounds, they need to be resistant to a variety of factors, including detergent activity [15]. Naphthol dye is a dye that is often used in the batik industry. This compound is not easily degraded and is a source of pollution in the environment with its carcinogenic and mutagenic properties. Some of the dangerous consequences that this compound causes in humans include increased heart rate, shock, cyanosis, eye irritation, respiratory problems, etc.

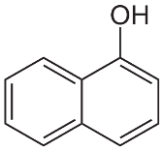

Figure 1. Molecular structure of naphthol[16]

This compound has an anionic (negatively charged) dye in the solution phase [16]. So the MIL-100(Fe)@Fe_3O_4 composite needs to be modified on its surface so that it can adsorb naphthol well.

CTAB (cetyltrimethylammonium-bromide) is a type of cationic surfactant made up of an amine group-attached cationic organoamine with a carbon chain tail and containing a hydrocarbon group (non-polar) and a hydrophilic group (polar) [17]. The structure of the CTAB surfactant is shown in Figure 2.

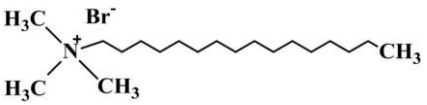

Figure 2. Molecular structure of CTAB

CTAB (cetyltrimethylammonium-bromide) is widely used as an adsorbent modification agent such as zeolite, bentonite, and silica, resulting in a positively charged surface [18]. Surface modification of the MIL-100(Fe)@Fe_3O_4 composite with CTAB was carried out with the aim that the naphthol compound as liquid waste from the batik industry could be effectively adsorbed by the composite.

2 MATERIALS AND METHODS

2.1 Instrumentation

The compound of Fe_3O_4, MIL-100(Fe), MIL-100(Fe)@Fe3O4 and MIL-100(Fe)@Fe_3O_4-CTAB composite were characterized by Fourier transform infrared spectrometer with brand 8400S Shimadzu and X-ray diffractometer with brand Philips X-Pert MPD. The concentration of naphthol, however, was ascertained using a UV-visible spectrophotometer.

2.2 Materials

The materials used in this study were zircon mining waste, 1-Naphthol (C.I. 822289; pro analysis by Merck), $FeSO_4.7H_2O$ (pro analysis by Merck), CTAB (pro analysis by Merck), HCl (pro analysis by Merck), H_3BTC (pro analysis by Merck), NH_4OH (pro analysis by Merck) and aquadest.

2.3 Zircon Mining Magnetic Waste Preparation

In order to separate zircon mining waste comprising magnetic and non-magnetic materials, samples of zircon sand waste processing were subjected to an external

magnetic field. After that, the sample that reacts to outside magnets was gathered and put through a 100-mesh screen until it was clear.

2.4 Synthesis of Fe_3O_4 from Magnetic Zircon Mining Waste

Six grams of the material were weighed, dissolved in sixty milliliters of strong hydrochloric acid (~12 M), and heated to eighty degrees Celsius for ninety minutes while being agitated with a magnetic stirrer. Next, two passes over ash-free filter paper were performed on the solution. After that, the filtrate was titrated using a 6.5 M NH_4OH solution until the solution's pH reached 9. To obtain the Fe_3O_4 precipitate at pH 10 and 11, the same process was used. After that, the precipitate was cleaned with distilled water, separated with the use of a magnetic field outside, and dried at 110 ^oC for three hours. The material was then examined using Fourier transform infrared spectrometer with brand 8400S Shimadzu and X-ray diffractometer with brand Philips X-Pert MPD.

2.5 Synthesis of MIL-100(Fe)@Fe_3O_4 Composite

The synthesis of MIL-100(Fe)@Fe_3O_4 composite is based on research that was carried out with a few changes by Tan and Foo (2021). A total of 3.8 grams (13.7 mmol) of $FeSO_4.7H_2O$ was dissolved in 120 mL of 0.01 M HCl to create MIL-100(Fe). 12.5 grams of Fe_3O_4 were then added as Solution A. Solution B consisted of dissolving 1.9 grams (9.1 mmol) of H_3BTC in 30 mL of 1 M NaOH (3 mmol) in a different container. After that, solution A was gradually added to solution B while being stirred with a magnetic stirrer at a speed of 200 rpm until all of the solution A had been reacted with. Subsequently, the reaction mixture was left to stand at room temperature for a full day while being constantly swirled at a speed of 200 revolutions per minute. This was done until the liquid steadily changed color from bluish green to brownish orange. After cooling the resultant solid to room temperature, it was cleaned three times with water and once with methanol before being dried for 12 hours at 60 ^oC [19]. Following the production of the MIL-100(Fe)@Fe_3O_4 composite, Fourier transform infrared spectrometer with brand 8400S Shimadzu and X-ray diffractometer with brand Philips X-Pert MPD were used to characterize the results.

2.6 Synthesis of MIL-100(Fe)@Fe_3O_4-CTAB Composite

In 25 milliliters of CTAB solution, the MIL-100(Fe)@Fe_3O_4 composite was distributed at different concentrations ranging from 0.1 to 0.7 M. For seventeen hours, the mixture was agitated using a magnetic stirrer. After being cleaned of Br-ions with distilled water, the resulting MIL-100(Fe)@Fe_3O_4-CTAB solid was dried at 80 °C in an oven. Using Fourier transform infrared spectrometer with brand 8400S Shimadzu and X-ray diffractometer with brand Philips X-Pert MPD., the produced MIL-100(Fe)@Fe_3O_4-CTAB adsorbent was investigated.

2.7 Investigation of Naphthol Adsorption in the Aqueous Phase

The MIL-100(Fe)@Fe_3O_4-CTAB composite adsorption investigation on naphthol dye was mostly conducted using a method in batches. By adjusting the initial the solution's pH (4, 5, 6, 7, 8, 9 and 10), the contact duration (t: 20, 40, 60, 80, 100, and 120 min), and the initial concentration of naphthol (Co; 50, 100, 150, 200, 250, 300, 350, and 400 mg/L), the impacts of various parameters on the adsorption process's rate were observed. The studies used 100 ml Erlenmeyer

flasks with 50 ml of naphthol inside that were shaken at 100 rpm for three hours at that point, at room temperature. The UV-Visible spectrophotometer was used to calculate the amount of naphthol that remained in each sample following adsorption.

To ascertain the naphthol adsorption kinetics in the aqueous phase, the adsorption process's kinetic parameters were examined for contact time. Next, the information was regressed against pseudo-second-order kinetics and first-order kinetics formulas. In contrast, the Freundlich and Langmuir models were used in this work to represent the real outcomes of adsorption isotherms.

3 RESULTS AND DISCUSSION

3.1 Synthesis and characterization

In this research, the materials Fe_3O_4, MIL-100(Fe), MIL-100(Fe)@Fe_3O_4, and MIL-100(Fe)@Fe_3O_4-CTAB were synthesized. Fe_3O_4 material is dark black, MIL-100(Fe) material is brown, and MIL-100(Fe)@Fe_3O_4 and MIL-100(Fe)@Fe_3O_4-CTAB materials have the same color, namely whitish brown. Fe_3O_4 material has the darkest color of all materials. Next, MIL-100(Fe) material has a dark brown color, with a hint of orange accompanying it. Fe_3O_4 material is in the form of coarse grains that do not combine with each other. Meanwhile, MIL-100(Fe) is in the form of a fine powder with a powder texture that blends together. However, the MIL-100(Fe)@Fe_3O_4-CTAB material has a whiter color than the MIL-100(Fe)@Fe_3O_4 material. (**Figure 3**).

(a) (b) (c) (d)

Figure 3. The synthesized of materials Fe_3O_4 (a), MIL-100(Fe) (b), MIL-100(Fe)@Fe_3O_4 (c), and MIL-100(Fe)@Fe_3O_4-CTAB (d)

The obtained Fe_3O_4, MIL-100(Fe), and MIL-100(Fe)@Fe_3O_4 were after which an FTIR spectrometer was used to check its functional groups. The infrared spectra of these materials are shown in **Figure 4**. Based on the the FTIR spectrum results, the Fe_3O_4 compound has the absorption peaks at the wavenumbers of 538 cm^{-1} and 443 cm^{-1} (**Figure 4(e)**), which are characteristic of Fe-O stretching vibration on tetrahedral sites (Fe^{2+} O^{2-}) and Fe-O on octahedral sites (Fe^{3+} O^{2-}), respectively [20]. Furthermore, the peak of absorption at 3447 cm^{-1} wavenumbers in **Figure 4(d)** of the MIL-100(Fe) spectrum represents the vibrational absorption of the O-H group and is caused by the MIL-100(Fe) sample's presence of both bound and free water. The stretching vibration of the C=O group is shown by the peak at wavenumber of 3447 cm^{-1}. The bending vibrations of the C-H group of the benzene ring from H_3BTC are represented by the peaks at 760 cm^{-1} and 710 cm^{-1}, while the stretching vibrations of the O-C-O group are represented by the peaks at 1449 cm^{-1} and 1382 cm^{-1}. Then, at a wavenumber of 460 cm^{-1}, the apex of the Fe-O stretching vibration appears [14].

Nearly identical to the MIL-100(Fe) sample's FTIR spectrum is the MIL-100@Fe_3O_4 sample's (**Figure 4(c)**). The

new peaks at wave numbers 3434 cm^{-1}, 1627 cm^{-1}, 1445 cm^{-1}, 459 cm^{-1}, and 763 cm^{-1}, respectively, are caused by the absorption of stretching vibrations of O-H, C=O, O-C-O, Fe-O, and bending vibrations of C-H groups. The MIL-100@Fe_3O_4 spectrum shows that the addition of Fe_3O_4 to the MIL-100 structure increases the amount of Fe-O bonds and decreases the interaction with free water, as seen by the comparatively low peak of the O-H group at 3434 cm^{-1} and the elevated peak of the Fe-O bond at 459 cm^{-1}.

The CTAB's FTIR spectrum displays absorption peaks at wavenumbers of 2856 and 2925 cm^{-1} (**Figure 4(b)**), corresponding to the C-H stretching modes in the 2800–3000 cm^{-1} range. The symmetric and antisymmetric CH_2 stretches are the source of the two prominent peaks at 2925 and 2856 cm^{-1}. Around 2900 cm^{-1}, the broad shoulder forms a resonance structure. The two unresolved components of the antisymmetric CH_3 stretch are responsible for the peak at 2960 cm^{-1}. The symmetric CH_3 stretch's resonance structure is estimated to be between 2880 and 2940 cm^{-1} [21, 23-24].

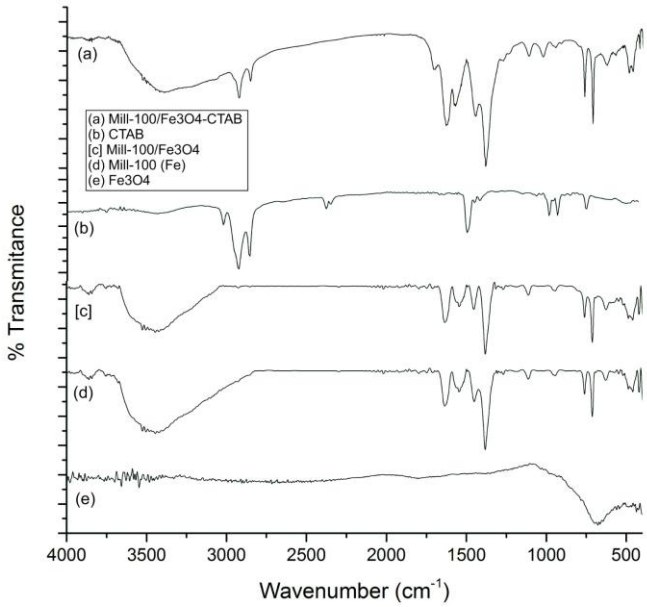

Figure 4. The FTIR spectra of MIL-100(Fe)@Fe_3O_4-CTAB (a), CTAB (b), MIL-100(Fe)@Fe_3O_4 (c), MIL-100(Fe) (d) and Fe_3O_4 (e)

The FTIR MIL-100@Fe_3O_4-CTAB spectrum has a combined spectrum between spectrum of MIL-100@Fe_3O_4 and spectrum of CTAB. The infrared spectra of these materials are shown in **Figure 5**. The MIL-100(Fe)@Fe_3O_4-CTAB composite has absorption peaks at wavenumbers of 3395, 2923, 2852, 1628, 1445, 1383, 1021, 763, 713, 621, and 482 cm^{-1} **(Figure 5)**. These are the absorption of bending vibrations of C-H groups and stretching vibrations of O-H, C-H, H-C-H, C=O, O-C-O, and Fe-O groups. There are several new peaks that are a result of the CTAB. From this spectrum, it can be clearly seen that CTAB is bound to the composite group. The FTIR spectrum's findings serve as the basis for these.

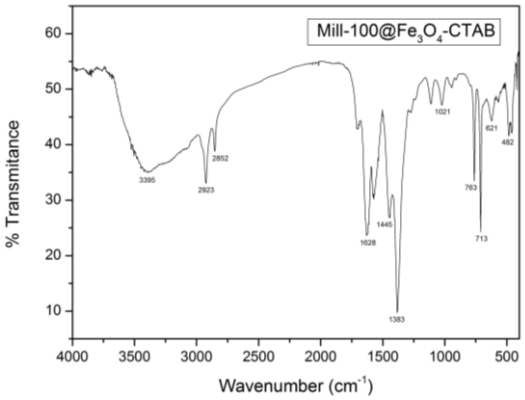

Figure 5. The FTIR spectra of MIL-100(Fe)@Fe_3O_4-CTAB

XRD confirmed the effective synthesis of the Fe_3O_4, MIL-100(Fe), MIL-100(Fe)@Fe_3O_4, and MIL-100(Fe)@Fe_3O_4-CTAB composite. **Figure 6** displays the X-ray diffractograms for the Fe_3O_4, MIL-100(Fe), MIL-100(Fe)@Fe_3O_4, and MIL-100(Fe)@Fe_3O_4-CTAB composite. Figure 6(d) shows that the samples evaluated in this investigation contain characteristic peaks for iron oxide of magnetite (Fe_3O_4) at 2θ of 30.143, 35.510, and 43.195, based on standards set by the Joint Committee on Powder Difraction (JCPDS; No. 19-629). The MIL-100(Fe) X-ray diffractogram likewise exhibits a pattern resembling that of the earlier study (CCDC No. 640536) at 2θ of 6.079; 10.217; 10.961; 12.486; 19.006; 20.035; 23.933; and 27.997, which employed synthesis techniques at room temperature **(Figure 3(c))**. Additionally, the diffactogram of the MIL-100(Fe)@Fe_3O_4 composite showed a significant degree of similarity with Fe_3O_4 (2θ = 30.134; 35.389; and 43.164) and MIL-100(Fe) (2θ = 10.07; 10.872; 19.958; 23.85; and 27.643) (Figure 3(b)).

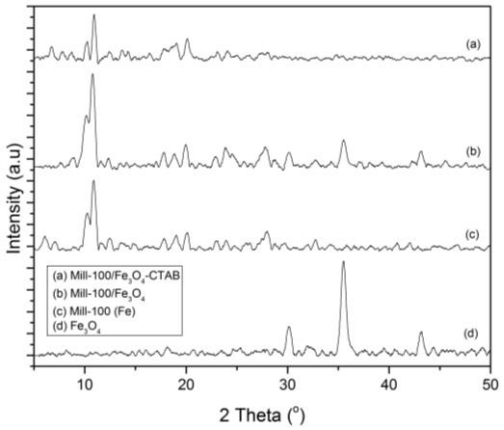

Figure 6. The XRD diffractograms of MIL-100(Fe)@Fe_3O_4-CTAB (a) MIL-100(Fe)@Fe_3O_4 (b), MIL-100(Fe) (c) and Fe_3O_4 (d).

XRD confirmed that the MIL-100(Fe)@Fe_3O_4-CTAB composite was successfully synthesized. Figure 7 displays the X-ray diffractograms of the MIL-100(Fe)@Fe_3O_4-CTAB composite. Typical peaks at 2θ of 6.68; 7.86; 10.24; 10.92; 13.70; 14.27; 19.06; 20.09; 23.05; 24.04 and 28.03 can be seen in the samples examined in this investigation, according to standards set by the Joint Committee on Powder Difraction (JCPDS: No. 75-0576) [22]. There are several new peaks that are a result of the CTAB. From this difactogram, it can be clearly seen that CTAB is bound into the composite group.

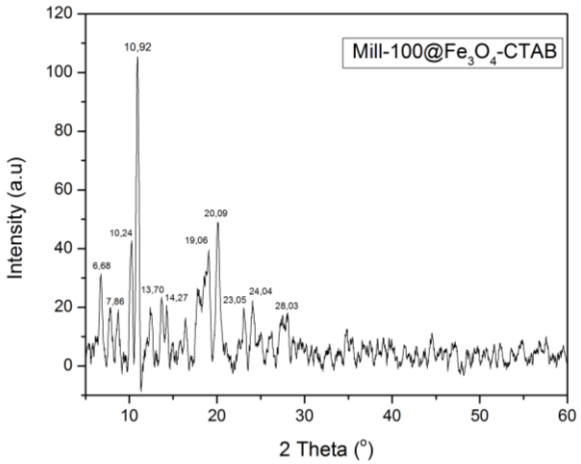

Figure 7. The XRD diffractograms of MIL-100(Fe)@Fe_3O_4-CTAB.

3.2 Results of Naphthol Adsorption in The Aqueous Phase

The effect of CTAB concentration on MIL-100(Fe)@Fe_3O_4-CTAB composite for naphthol adsorption can be seen in **Figure 8**. CTAB variations were carried out to determine the most optimal form of composite for adsorbing naphthol dyes. From this research, it is known that the most optimal CTAB concentration is 0.4 M. When the CTAB concentration is increased to more than 0.4 M, the composite will be in a stable state of adsorption (**Figure 9**). This is because CTAB no longer has a place to bond with the MIL-100(Fe)@Fe_3O_4 composite. In other words, the CTAB compound no longer has any groups in the composite to attach to.

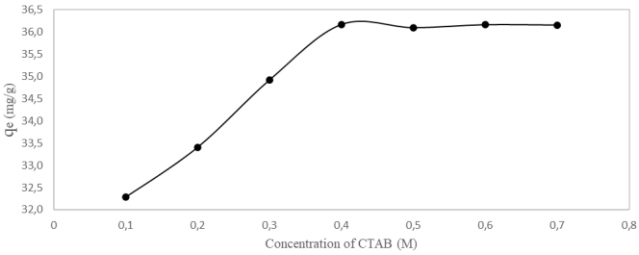

Figure 8. The effect of CTAB concentration on MIL-100(Fe)@Fe_3O_4-CTAB

The impact of pH on MIL-100(Fe)@Fe_3O_4-CTAB's adsorption capability on naphthol can be seen in **Figure 9**. The adsorption ability of the adsorbent is good at comparatively low pH values, where the pH optimum for the adsorption process was 6. This shows that the adsorption process will run optimally when the solution has a relatively acidic pH. The results show

that the adsorption process by MIL-100(Fe)@Fe_3O_4-CTAB composite begins to occur significantly at pH 4-10. The optimal pH for the composite to adsorb naphthol dye is 6. This is because the MIL-100(Fe)@Fe_3O_4-CTAB composite basically has a positive charge. So it will be easier to adsorb naphthol dyes under acidic conditions. In acidic conditions, the solution will be filled with protons (H^+), which will increase the adsorption process of naphthol dye, whereas naphthol has a negative charge.

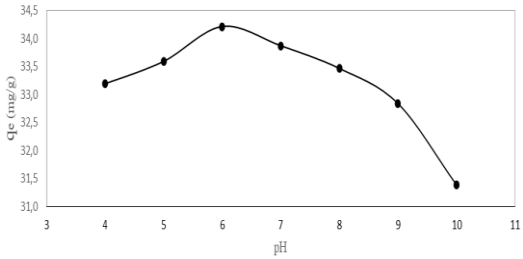

Figure 9. The impact of pH on MIL-100(Fe)@Fe_3O_4-CTAB's adsorption capability

Figure 10 shows the impact of contact time on the adsorption capacity (q_e) of the MIL-100(Fe)@Fe_3O_4-CTAB composite on naphthol. At low contact time (under 20 minutes) will also produce a low adsorption process. This is because not all of the naphthol has been adsorbed into the adsorbent. At high contact times (above 80 minutes), the adsorption process will be stable and even relatively decreased. This is because the naphthol that was previously adsorbed in the adsorbent can then be free and dissolve into the solution. The naphthol adsorption on the adsorbent demonstrates, according to the data, that an ideal contact period for adsorption is 80 minutes. Furthermore, the findings indicate that comparatively significant amounts of naphthol are adsorbed in the early going and eventually tend to approach equilibrium.

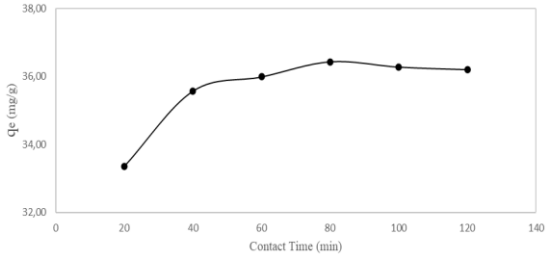

Figure 10. The impact of contact duration on MIL-100(Fe)@Fe_3O_4-CTAB's adsorption capability

The first-order kinetics and pseudo-second-order kinetics equations were then used to regress the data (Figure 11). These graphs were used to compute the correlation coefficient (R^2), which measures how applicable each model is. These plots' linearity suggests that both models are applicable. The pseudo-second-order model matches the experimental data more closely than the pseudo-first-order model, according to the correlation coefficient finding ($R^2 > 0.700$; $R^2 > 0.999$).

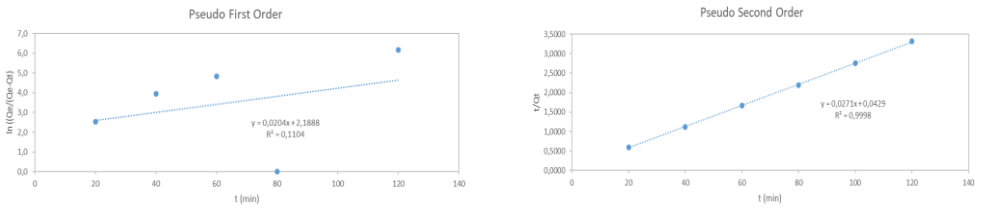

(a) (b)

Figure 11. Curves representing naphthol's pseudo first order (a) and pseudo second order (b) kinetics

With respect to the adsorption mechanism, chemisorptions are indicated by the adsorption kinetics model, which also demonstrates that the square of the naphthol concentration determines the adsorption rate, represented by $(q_e-q_t)^2$. Table 1 displays the kinetic parameters' outcome values.

Table 1. Adsorption kinetics models for naphthol

Materials	Pseudo 1st Order		Pseudo 2nd Order	
	β (min^{-1})	R^2	k_2 (g/mg.min)	R^2
MIL-100(Fe)@Fe_3O_4-CTAB	0,0204	0,1104	1,712 x 10^{-2}	0,9998

Figure 12 illustrates how changes in naphthol concentration affect the MIL-100(Fe)@Fe_3O_4-CTAB composite's adsorption capacity. At a low concentration of naphthol (below 250 ppm), it will also produce a low adsorption process. This is because there is a lot of adsorbent remaining in the solution while the naphthol has all been adsorbed into the adsorbent. At high concentrations of naphthol (above 250 ppm), a stable adsorption process will result. This is because all the adsorbents are already at their maximum adsorption capacity and no adsorbents are dissolved in the solution. The findings indicate that naphthol adsorption on adsorbents reaches its peak capacity around 250 ppm, following it tends to become closer to balance before declining as concentration rises.

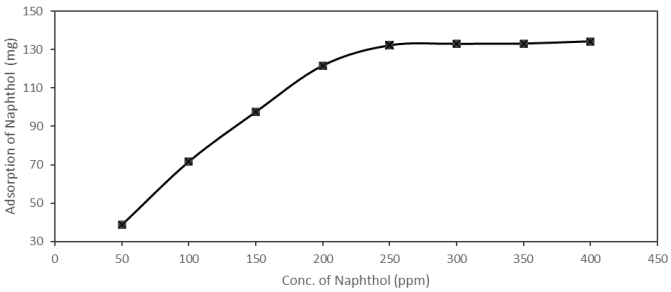

Figure 12. The impact of naphthol concentration on MIL-100(Fe)@Fe_3O_4-CTAB adsorption ability

Adsorption energy, adsorption capacity, and adsorption equilibrium are all determined by adsorption equilibrium. How much material is adsorbed and how much the substance's concentration is at equilibrium by the adsorbent is described by the isotherm pattern. To gain further insight into the correlation between the naphthol adsorption isotherm and the experimental

data, two-parameter isotherm models—Langmuir and Freundlich—were also used to evaluate the data. The outcomes are displayed in **Figure 13**.

These graphs were used to compute the correlation coefficient (R^2), which measures how applicable each model is. These plots' linearity suggests that the model is applicable. The correlation coefficient, as indicated by the result, demonstrates that the Isoterm Freundlich model (R^2=0.9456) fits the experimental data less well than the Isoterm Langmuir model (R^2=0.9992).

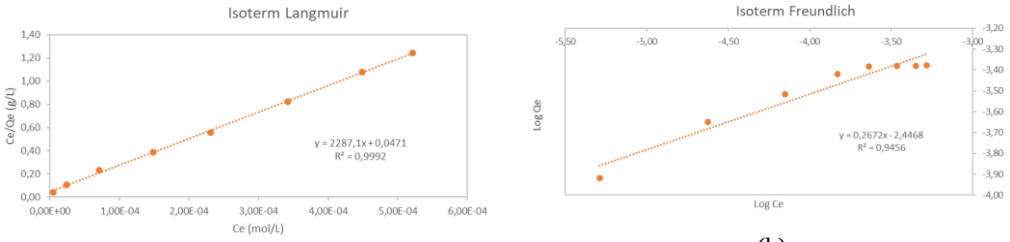

(a) (b)

Figure 13. Curves of the naphthol adsorption Isoterm Langmuir model (a) and Isoterm Freundlich model (b)

It may be inferred from the comparison of R^2 values that the Langmuir adsorption equation is followed by the naphthol adsorption on MIL-100(Fe)@Fe_3O_4-CTAB composite, since the Langmuir isotherm model's equation has an R^2 value of 0.9992, which is closer to 1. According to this hypothesis, chemisorption or strong electrostatic interactions are responsible for naphthol's adsorption on the adsorbent surface**.** **Table 2** displays the equilibrium parameter outcome values for the two isoterm models.

Table 2. Equilibrium kinetics models for naphthol

Materials	Isoterm Langmuir				Isoterm Freundlich		
	B (mg/g)	K (L/mol)	E (kJ/mol)	R^2	B (mg/g)	N	R^2
MIL-100(Fe)@Fe_3O_4-CTAB	63.036	48558.39	26.64	0.9992	3.574×10^{-3}	3.743	0.9456

The adsorption capacity (B) of naphthol on the MIL-100(Fe)@Fe_3O_4-CTAB composite may be calculated using the Langmuir isotherm model, as seen in Table 2. The adsorption capacity (B) of the MIL-100(Fe)@Fe_3O_4-CTAB composite is 63.036 mg/g for naphthol, respectively. The adsorption energy can be found using the Langmuir isotherm model and the formula E = RT ln K. The computation results indicate that 26.64 kJ/mol of energy is needed for naphthol adsorption on the MIL-100(Fe)@Fe_3O_4-CTAB composite. This indicates that electrostatic interaction between the two adsorbents and naphthol occurs. Because naphthol is positively charged and the active sites of the MIL-100(Fe)@Fe_3O_4-CTAB compound are positively charged, electrostatic bonding takes place.

4 CONCLUSION

In this study, Iron precursors from magnetic waste from zircon mining were successfully used to create a magnetite composite (Fe_3O_4) with comparatively high yields. Then, a batch technique was employed to remove naphthol from the aqueous phase utilizing the synthesized MIL-100(Fe)@Fe_3O_4-CTAB composite. For adsorption, 0.4 M is the ideal concentration of CTAB. At pH 6, the highest amount of dye removed from the adsorbent was achieved. The rate constant values for MIL-100(Fe)@Fe_3O_4-CTAB were 1,712 x 10^{-2} g/mg.menit, respectively, and the adsorption kinetics were governed by a pseudo second-order kinetics model. Additionally, the data demonstrated that the Langmuir isotherm for adsorption capacity of 63.036 mg/g is followed by the adsorption isotherm model of MIL-100(Fe)@Fe_3O_4-CTAB. The outcome demonstrates that the MIL-100(Fe)@Fe_3O_4 composite can enhance its capacity for naphthol adsorption while also making the process of separating the adsorbent solid easier.

CONFLICT OF INTEREST

The writers claim that there isn't a conflict of interest. Because the author completed the research to the best of his abilities, worked in a cohesive team, and processed all available references.

ACKNOWLEDGEMENTS

The author provides appreciation to Universitas Palangka Raya's Lembaga Penelitian dan Pengabdian kepada Masyarakat for a research grant in 2023, contract number 0713/UN.24.13/AL.04/2023. The author would like to thank the BIO publisher, who has helped this article be published as a proceeding.

REFERENCES

1. H. Suprihatin, Pus. Penelit. Lingkung. Hidup Univ. Riau 130 (2014)
2. R. Kant, Nat. Sci. **04**, 22 (2012)
3. R. Azhar, D. Tuwohingide, D. Kamudi, Sarimuddin, and N. Suciati, Procedia Comput. Sci. **72**, 24 (2015)
4. N. Hasaniyah and H. Basri, Proceeding Int. Conf. Eng. Technol. Soc. Sci. **1**, 39 (2020)
5. W. Sutari, Y. N. D. Yekti, M. D. Astuti, and Y. M. sari, Procedia Manuf. **4**, 133 (2015)
6. L. S. Usop and T. B. Usop, Mudra J. Seni Budaya **36**, 405 (2021)
7. I. M. Sadiana, K. Karelius, R. Agnestisia, and A. H. Fatah, Molekul **13**, 63 (2018)
8. T. Rahayuningsih, F. S. Rejeki, E. R. Wedowati, and D. Widhowati, IOP Conf. Ser. Earth Environ. Sci. **475**, 0 (2020)
9. M. W. Kurniawan, P. P. -, and S. S. -, J. Ilmu Lingkung. **11**, 62 (2014)
10. S. Kumar, W. Ahlawat, G. Bhanjana, S. Heydarifard, M. M. Nazhad, and N. Dilbaghi, J. Nanosci. Nanotechnol. **14**, 1838 (2014)
11. S. E. Rizk and M. M. Hamed, Desalin. Water Treat. **56**, 1536 (2015)
12. W. Dai, H. Yu, N. Ma, and X. Yan, Korean J. Chem. Eng. **32**, 335 (2015)
13. N. A. H. M. Nordin, A. F. Ismail, A. Mustafa, P. S. Goh, D. Rana, and T. Matsuura, RSC Adv. **4**, 33292 (2014)
14. S. Huang, K. L. Yang, X. F. Liu,

H. Pan, H. Zhang, and S. Yang, RSC Adv. **7**, 5621 (2017)

15. M. T. Yagub, T. K. Sen, S. Afroze, and H. M. Ang, Adv. Colloid Interface Sci. **209**, 172 (2014)
16. A. A. Ali, S. R. El-Sayed, S. A. Shama, T. Y. Mohamed, and A. S. Amin, Desalin. Water Treat. **204**, 124 (2020)
17. M. E. Mahmood and D. a F. Al-koofee, Glob. J. Sci. Front. Res. Chem. **13**, 1 (2013)
18. S. R. Taffarel and J. Rubio, Miner. Eng. **23**, 771 (2010)
19. K. L. Tan and K. Y. Foo, J. Environ. Chem. Eng. **9**, 104923 (2021)
20. V. Rathod, A. V. Anupama, R. V. Kumar, V. M. Jali, and B. Sahoo, Vib. Spectrosc. **92**, 267 (2017)
21. R. A. Campbell, S. R. W. Parker, J. P. R. Day, and C. D. Bain, Langmuir **20**, 8740 (2004)
22. X. M. Sun, X. Chen, Z. X. Deng, and Y. D. Li, Mater. Chem. Phys. **78**, 99 (2003)
23. Y. Rilda, P. V. P. Ayuni, R. Refinel, A. Armaini, A. Agustien, A. Almurdi, and H. Pardi, Rasayan J. Chem. **15**, 402 (2022)
24. Y. Rilda, E. S. Putra, S. Arief, A. Agustien, H. Pardi, and N. Sofyan, J. Dispers. Sci. Technol. **0**, 1 (2023)